Barstar Has a Highly Dynamic Hydrophobic Core: Evidence from Molecular Dynamics Simulations and Nuclear Magnetic Resonance Relaxation Data†

Kam-Bo Wong‡ and Valerie Daggett*

Department of Medicinal Chemistry, University of Washington, Seattle, Washington 98195-7610

Received March 11, 1998; Revised Manuscript Received May 14, 1998

ABSTRACT: The dynamic behavior of the ribonuclease inhibitor barstar has been investigated by molecular dynamics (MD) simulations in explicit water. Two 2.5 ns MD simulations were performed, and an ensemble of 25 000 structures was generated. This ensemble reproduces the solution structures and is consistent with the experimental structural restraints from NMR spectroscopy. Reorientation of the backbone NH bond vectors and side chain methyl groups was monitored by calculation of autocorrelation functions and the generalized S^2 order parameters. Order parameters derived for motion in the ∼100 ps time scale were compared with those obtained from NMR relaxation measurements. Consistent with experiment, the backbone NH bond vectors were relatively rigid. In contrast, the side chain methyl groups exhibited a wide dynamic range, from restricted motion comparable to that of the backbone to rapid unrestricted motion. The order parameters for the methyl groups correlate well with their spatial separation from the backbone and are residue-type dependent. Smaller S^2_{axis} values were observed for leucine methyl groups, in part due to side chain hopping between two predominant rotamers (g^+t and tg^-). Motions such as the flipping of aromatic rings and the hopping of leucine side chains were prevalent within the hydrophobic core, suggesting that the core is fluid-like with low energy barriers between native conformational substates. Thus, our studies suggest that the entropy of the native state can be significant and should not be discounted in thermodynamic considerations of protein folding. On the basis of our results, the side chain motion represents the primary source of the residual entropy of the native state and entropic considerations based solely on backbone dynamics would be incomplete.

Proteins in solution are not static but instead experience a wide range of dynamic behavior in terms of the amplitude of the motion, the distribution of the motion within the protein, and the time scale of the motion. Atomic coordinates obtained from X-ray crystallography and NMR spectroscopy only represent an average view of a protein. Elucidation of the dynamic behavior of proteins in solution is necessary for a complete understanding of protein stability and function. Recent advances in NMR spectroscopy are making high-resolution studies of protein dynamics possible [reviewed by Palmer (*1*) and Wagner (*2*)]. Most studies thus far have focused on backbone amide dynamics of ^{15}N-labeled protein samples (*1*−*4*, and references therein); however, there are an increasing number of studies and methodological developments in the areas of side chain dynamics utilizing ^{13}C- and ^{2}H-labeled samples (*5*−*9*). Even given these advances, it is generally difficult to extract detailed and comprehensive atomic information directly from the experimental results. Molecular dynamics (MD) simulations, in this regard, complement experimental studies by providing structural models over time to aid in the interpretation and representation of the empirical data. In the limit of the present computational power, MD simulations are ideally suited for the study of protein motion on the time scale of picoseconds to nanoseconds, which falls nicely into the time scale of motions described by NMR relaxation measurements.

Barstar is a good system for the study of protein dynamics by MD simulations. It is a small protein with 89 residues. Its structure has been solved by NMR spectroscopy (*10*, *11*) and X-ray crystallography (*12*, *13*). It is an α and β protein with four helices and a three-stranded β-sheet (Figure 1). Most importantly, backbone ^{15}N relaxation data are available (*11*), allowing comparison of the experimental data with the predictions from the MD simulations.

Barstar is an intracellular inhibitor of the ribonuclease barnase from *Bacillus amyloliquefacien*. Barstar and barnase form a 1:1 complex, blocking the active site of barnase (*12*, *13*). Regions of barstar that bind to barnase are mainly localized in the binding loop (Pro 27−Glu 32) and helix 2 (Figure 1). ^{15}N relaxation studies of barstar suggest that while backbone motion on a sub-nanosecond to picosecond time scale is relatively restricted, slow conformational exchange on a microsecond to millisecond time scale is substantial (*11*). Here we simulate the solution structure of barstar by performing simulations at 298 K in explicit water. Time correlation functions and order parameters for backbone NH vectors were derived from an ensemble of MD-generated structures over 5 ns, which oversamples motions in the sub-nanosecond time scale and allows for a quantitative comparison with the NMR relaxation data. Indications of motions slower than the nanosecond time scale were made

† This work was supported by the National Institutes of Health (Grant GM 50789).

* To whom correspondence should be addressed.

‡ Present address: Department of Chemistry, University of Cambridge, Lensfield Road, Cambridge CB2 1EW, U.K.

S0006-2960(98)00552-2 CCC: $15.00
Published on Web 07/21/1998

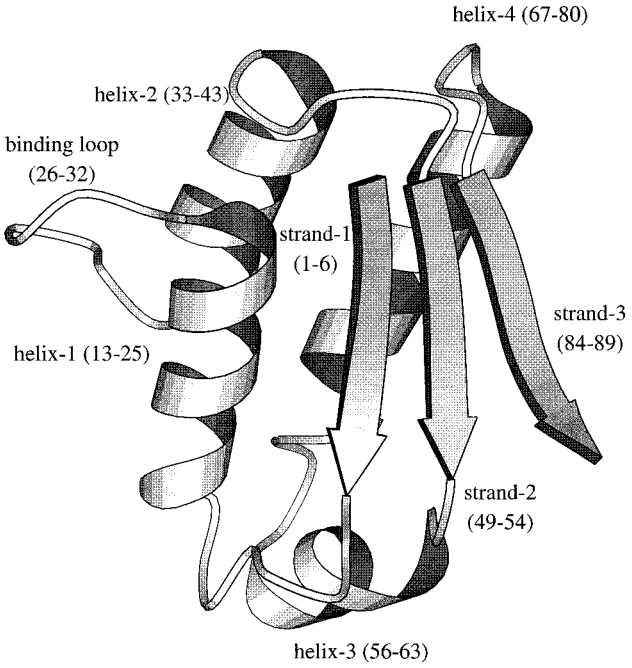

FIGURE 1: Ribbon representation of barstar with secondary structure elements indicated. Barstar consists of four α-helices and a three-stranded β-sheet. Residues that are important for interactions with barnase are mainly localized in the binding loop (residues 26−32) and helix 2 (residues 33−43) (*12*, *13*). This figure was created with MOLSCRIPT (*52*).

on the basis of a qualitative interpretation of order parameters derived from the MD simulations by comparing the degree of motion over short (250 ps) and longer (5 ns) time periods. We also report the side chain dynamics by following the reorientation of the symmetry axis of the methyl groups. Side chains in the core of barstar were found to experience a wide range of dynamic behavior, ranging from restricted motion comparable to that of the backbone to rapid unrestricted motion. Possible implications of the dynamic behavior on the stability and function of barstar are discussed.

METHODS

Molecular Dynamics Simulations. Molecular dynamics simulations were performed using the program ENCAD (*14*). An all-atom representation, including all hydrogens for protein and solvent, was employed, and the potential energy function and its implementation are described elsewhere (*15*, *16*). The starting structure for the simulation (structure number 130) was chosen randomly from the ensemble of NMR structures of C40/82A barstar (*11*) that have no violations of the experimental restraints. The ionization of charged residues was set to mimic a neutral pH environment (Asp and Glu residues were ionized, Lys and Arg were protonated, and His was neutral). The protein was first minimized for 500 cycles to relieve any bad contacts. Water molecules were added to fill a rectangular water box with walls at least 10 Å away from any protein atom. The density of the solvent was set to the experimental value of 0.997 g/mL at 298 K (*17*). Two separate MD simulations were performed. In one of the simulations (MD1), six sodium ions were added to yield an electrically neutral system while MD2 did not contain counterions. To prepare the solvent for MD, 8000 cycles of conjugate gradient minimization were performed on the solvent molecules, followed by 20 ps of MD at 298 K and a further 5000 cycles of minimization. The protein was then minimized for 5000 cycles, followed by 5000 cycles of conjugate gradient minimization and 5000 cycles of steepest descent of the full protein and solvent system. Atoms were then randomly assigned velocities according to a Maxwellian distribution. The temperature of the system was raised to 298 K by scaling velocities intermittently (it took ∼35 ps to reach 298 K). Periodic boundary conditions were applied, and the box volume was kept constant during the simulation. A nonbonded cutoff of 10 Å was used, and the nonbonded list was updated every five iterations. MD was performed using a 0.002 ps time step for 1.25×10^6 steps per simulation, resulting in two 2.5 ns trajectories. Structures were saved every 0.2 ps for analysis, generating an ensemble of 25 000 structures.

Comparison with NMR Relaxation Data. Rates of NMR relaxation are related to the autocorrelation function $C(t)$ of interatomic vectors (*19*). If the overall rotational diffusion and internal motions are independent, then $C(t)$ can be defined with $C(t) = C_r(t)C_i(t)$, where $C_r(t)$ and $C_i(t)$ are the rotational and internal motions, respectively. In the analysis of MD simulations, the contribution from rotational and translational diffusion is removed by superimposing structures to a common frame of reference. This was accomplished by computing the optimal superposition of all atoms using the method of Kabsch (*18*). Then, for the reorientation of the NH bond vectors, $C_i(t)$ is given by (*19*)

$$C_i(t) = \langle P_2[\mu(t')\mu(t'+t)]\rangle \quad (1)$$

where $\mu(t')\mu(t'+t)$ is the projection of a unit vector pointing along a NH vector at time t' and onto itself at a later time t, $P_2(x) = (^3/_2x^2 - {}^1/_2)$ is the second Legendre polynomial, and the broken brackets denote an ensemble or time average over the trajectory. $C_i(t)$ was calculated for 87 backbone NH vectors in both MD trajectories.

The generalized order parameter S^2 is defined as the long time limit of $C_i(t)$

$$S^2 = \lim_{t\to\infty} C_i(t) \quad (2)$$

For an MD simulation of finite length, T, S^2 can be obtained with (*20*)

$$S^2 = \frac{1}{T^2}\sum_{i=0}^{T}\sum_{j=0}^{T} P_2[\mu(i)\mu(j)] \quad (3)$$

where $\mu(i)\mu(j)$ is the projection of unit vectors along an NH bond at times i and j. If the pooled ensemble of both trajectories (MD1 and MD2) is considered, T is equal to 5 ns. In a second approach, order parameters were calculated with eq 3 with a window size T of 250 ps. An averaged S^2(250 ps) was obtained by sliding the window through time. Straight averaging of 250 ps slices of the trajectories gives the same results as the sliding window.

The dynamic behavior of the side chain methyl groups was monitored by following the reorientation of the symmetry axis of the CH_3 group. For example, the $C_\alpha - C_\beta$ axis is monitored for the methyl group of alanine. The autocorrelation function $C_{axis}(t)$ and order parameters S^2_{axis} for the

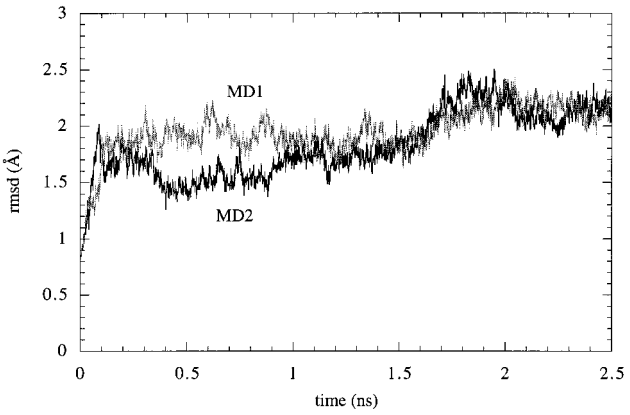

FIGURE 2: C_α root-mean-square deviation from the starting structure as a function of time for two MD simulations of barstar at 298 K.

symmetry axis of the methyl groups were calculated using eqs 1 and 3. A total of 58 methyl symmetry axes were monitored.

RESULTS

Structural Properties of Barstar in Solution

Two 2.5 ns MD simulations of barstar C40/82A were performed at 298 K. The C40/82A mutant, instead of wild-type barstar, was simulated because it has been the subject of NMR experiments and the mutations do not affect the structure (*11*). The same protocols were used for both simulations, except that one simulation contained six sodium ions to yield an electrically neutral system, while the other did not contain counterions. The sodium ions were very mobile, freely diffused around the solvent box, and appeared to have little effect on the protein.

The C_α root-mean-square deviation (rmsd) from the starting NMR structure is shown in Figure 2. The rmsd for both simulations was around or below 2 Å. Some representative snapshots from the MD-generated ensembles are displayed in Figure 3 (MD1, blue; and MD2, green). These structures are essentially superimposable with the ensemble of NMR-derived model structures (Figure 3, red). A more direct comparison with the NMR observables can be made by calculating the interproton distances contributing to the nuclear Overhauser enhancement cross-peaks (NOEs). Experimentally, an NOE is an average over an ensemble of $\sim 10^{18}$ structures and over time (milliseconds). Due to the nature of r^{-6} averaging, an infrequent contact between protons in a large ensemble can give rise to an NOE. Therefore, we do not expect all NOEs to be observed in MD simulations that last only 2.5 ns. In fact, however, most of the experimental NOEs are conserved in the simulation. The number of NOE violations is listed in Table 1. The number of violations decreased when the two trajectories were pooled, suggesting that better sampling of conformational space is obtained by combining individual simulations. Considering that there was not a major structural change during the MD simulations compared to the NMR ensemble, the simulations are reasonable models for the structural properties of barstar in solution. In the following analysis, the structures from the two simulations are pooled, analyzed, and treated as a single ensemble representative of the solution structure of barstar.

Dynamic Behavior of Barstar in Solution

Comparison of Simulated Main Chain Motion with the NMR-Generated Ensemble and Crystallographic Temperature Factors. As discussed above, rms deviations can be

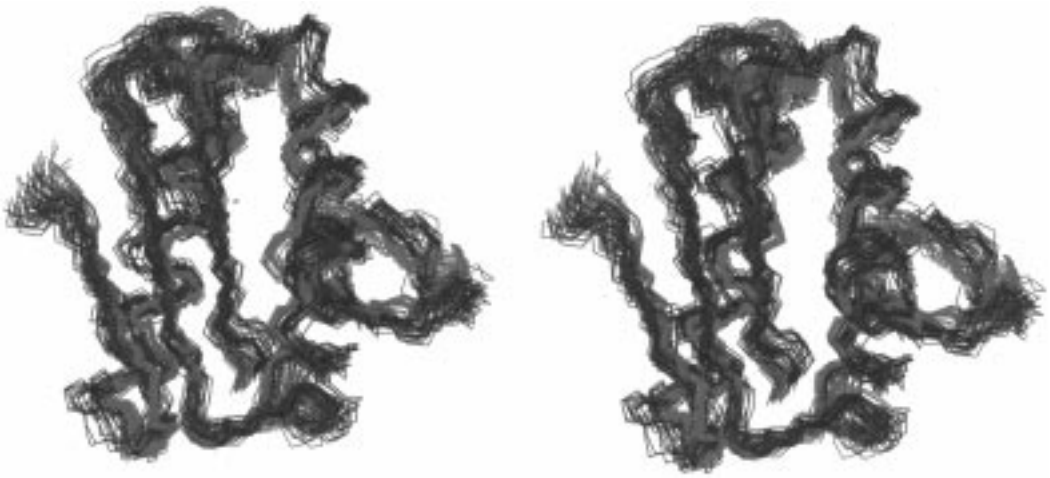

FIGURE 3: Snapshots of structures taken every 100 ps along the 2.5 ns trajectories from MD1 (blue) and MD2 (green) superimposed on the ensemble of NMR solution structures (red; PDB code 1ab7). This figure was created with MOLMOL (*53*).

Table 1: Summary of NOE Violations for the MD Simulations[a]

	<0.5 Å	0.5−1 Å	1−2 Å	2−3 Å	3−4 Å	4−5 Å	>5 Å
MD1	1411	51	47	10	4	0	0
MD2	1402	48	55	13	3	2	0
MD1 and MD2	1427	41	47	6	2	0	0

[a] Averaged interproton distances were calculated using $\langle r^{-6} \rangle^{-1/6}$ from ensembles of MD-generated structures and were compared to the upper bound of interproton distances predicted by the experimental NOEs (*11*). The upper bounds were set to 5.0 Å for all experimental NOEs. For NOEs involving methyl groups, 0.5 Å per interacting methyl group was added to the upper bounds to reflect the fact that methyl NOEs can be observed for proton pairs separated by longer distances. A total number of 1523 interproton distances were monitored, and most of them have violations of <0.5 Å.

used to assess how a protein evolves over the course of a simulation with respect to the starting structure. However, such deviations tell us little about the internal motion of the protein. In this regard, C_α root-mean-square fluctuations (rmsfs) are useful because they describe the motion about the mean conformation and reflect the flexibility of the protein chain. Large variations of the rms fluctuations were observed across the primary sequence, ranging from 0.5 to 1.6 Å, with the greatest mobility in the loop and turn regions (Figure 4A).

The rms fluctuations from the MD simulations can be compared with those derived from the ensemble of NMR solution structures. We note that the rms fluctuation from the average NMR structure depends on the number of restraints used for structural determination and is, at best, only an indirect indication of mobility. A more rigorous analysis of dynamics should be based on NMR relaxation parameters, which we discuss below. Nevertheless, the rms fluctuations for the NMR family of structures are consistent with the MD-derived values with higher fluctuations observed in loop and turn regions.

The crystallographic *B* factors represent the spread of the electron density and provide a rough measure of the mobility of the protein in the crystalline environment. The rmsf was calculated from the experimental temperature factors, *B*, from the crystal structure of barstar bound to barnase with rmsf $= (3/8\pi^2)B$. The regions of barstar that interact with barnase have low mobility in the crystal structure (Figure 4C). Thus, the binding loop and helix 2, which are very mobile in the free form, lose flexibility upon binding to barnase (compare panels A−C of Figure 4), as would be expected. Unfortunately, however, such a comparison is far from definitive because other factors contribute to the magnitude of the rmsf for the NMR and crystal structures.

Comparison with Backbone NMR Relaxation Data. Comparison with NMR relaxation data provides a better and more direct test of the magnitude of the motion simulated. Reorientation of NH vectors with respect to the external magnetic field, described by the angular autocorrelation function $C(t)$, provides a mechanism for ^{15}N relaxation (*21*). In an attempt to compare dynamic behavior from MD simulations to that probed with ^{15}N relaxation experiments, we have derived the angular autocorrelation functions for all backbone NH vectors. If we assume that internal motion is independent of the overall tumbling, $C(t)$ can be factored as $C(t) = C_r(t)C_i(t)$, where $C_r(t)$ and $C_i(t)$ are correlation functions for overall rotational tumbling and internal motions, respectively. Structures from the trajectories are superimposed on the starting structure to remove contributions from rotational and translational motions. This procedure is in theory similar to the model-free analysis and yields $C_i(t)$ for internal motions (*19*, *22*).

For all residues, $C_i(t)$ drops rapidly, within picoseconds, to about 0.8−0.9. This behavior corresponds to the ultrafast sub-picosecond librational motion of the NH vectors exhibited by essentially all proteins. $C_i(t)$ plots for some representative residues are shown in Figure 5A. For residues in regular secondary structure (e.g., Leu-41, helix 2), $C_i(t)$ drops rapidly to approximately 0.9 within a picosecond and remains at a high asymptotic value, corresponding to a high-order parameter. This finding indicates that the NH vectors are very ordered on a picosecond time scale. For residues in a loop, e.g., Trp 44, motion on the picosecond time scale is notable and the autocorrelation function levels off at a lower value. This is a result of less restricted motion of the NH groups in the loop regions. The NH vectors for some residues experience infrequent transitions (see Figure 5B), and in these cases, $C_i(t)$ will not decay to an asymptotic value.

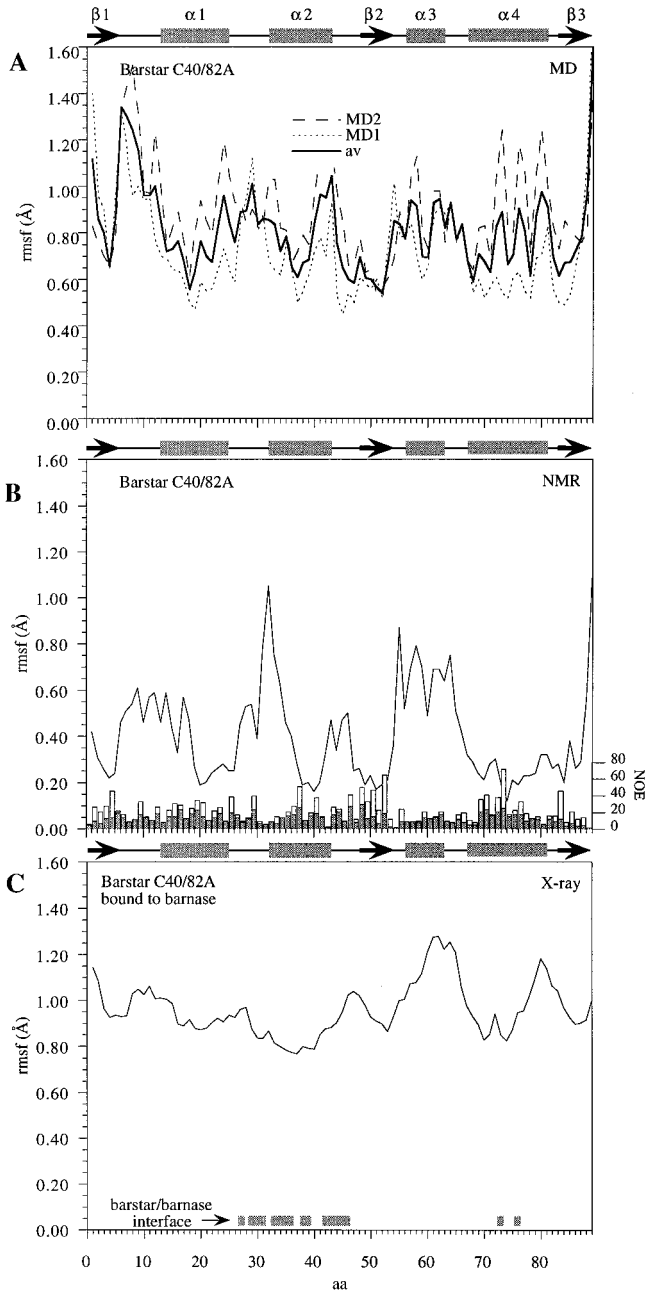

FIGURE 4: C_α root-mean-square fluctuation derived from (A) the MD-generated ensemble of structures, (B) the ensemble of NMR solution structures, and (C) the crystal structure of the barstar−barnase complex. The rms fluctuation by MD is the average rms deviation of individual structures during the simulation from the average structure for the simulation. This measure reflects the degree of motion experienced by the main chain during the simulation. For the NMR structures, the rms fluctuation is calculated in the same way, but only 20 structures are considered compared to 25 000 for MD. The values for the crystal structure are calculated from the *B* factors as described in the text. The position of the helices (boxes) and β-strands (arrows) is shown on the top of each panel. In panel B, the number of short-range ($1 \leq |i - j| \leq 4$) and long-range ($|i - j| \geq 5$) NOEs are shown as gray and white bars, respectively. In panel C, residues in the barstar−barnase interface are indicated.

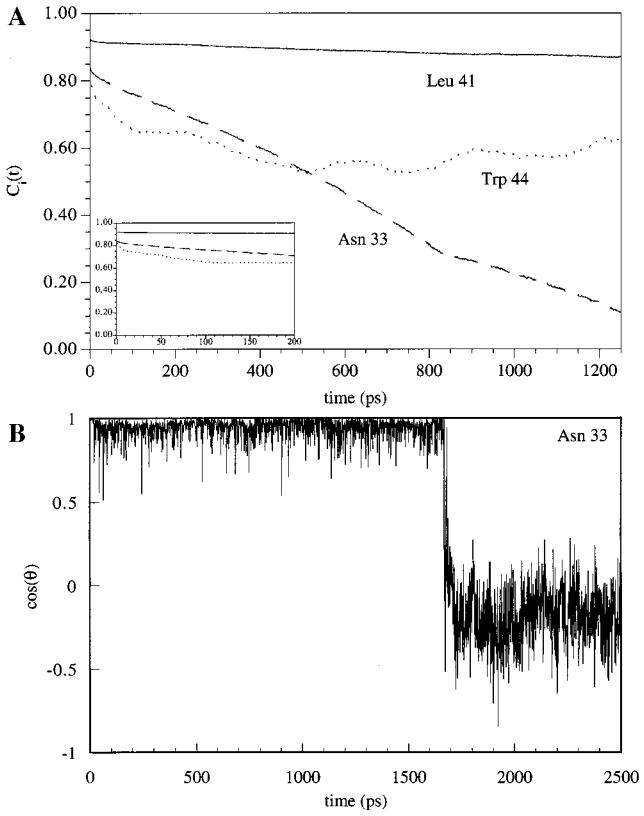

FIGURE 5: (A) Autocorrelation functions for representative backbone NH bond vectors. Asn 33 is the N-terminal residue of helix 2. Leu 41 is located in helix 2, and Trp 44 is in a loop region. (B) Orientation of the NH bond vector of Asn 33 as a function of time, where θ is the angle of the bond vector relative to its orientation at the beginning of the MD simulations. A transition is evident at approximately 1700 ps.

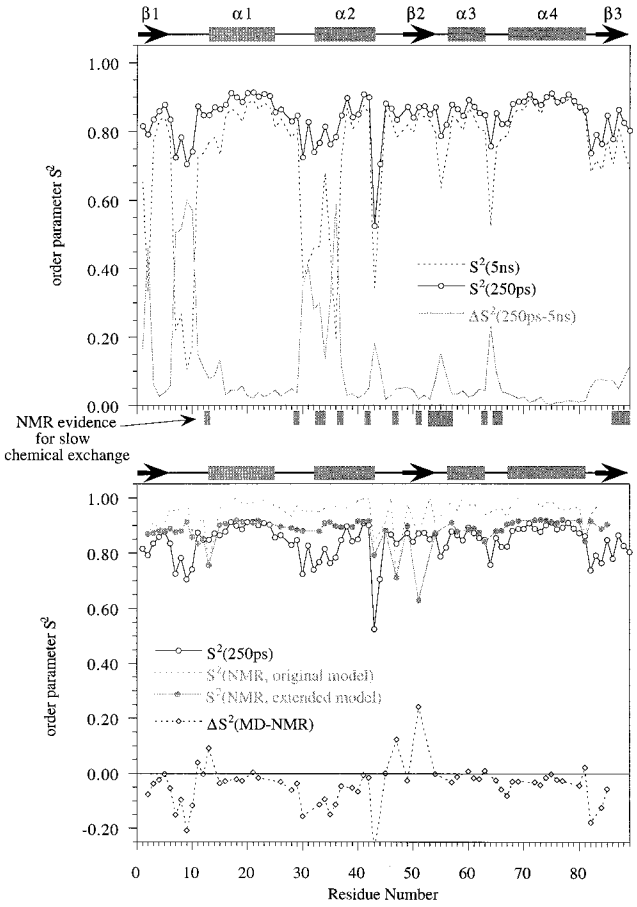

FIGURE 6: (A) MD-derived order parameters S^2 for backbone NH vectors. S^2 values were derived with eq 3 using two different window sizes: $T = 5$ ns (dotted line) and $T = 250$ ps (solid line). The differences between the two S^2 values (gray line) are indicative of motion slower than the ~100 ps time scales and are compared with the NMR evidence for slow chemical exchange. (B) Comparison of the MD-derived order parameters with those obtained from NMR experiments. Experimental S^2 values were derived from the original model-free analysis (*19*, *22*) and the extended model (*4*) are shown as gray lines. The difference between the S^2(250 ps) values from the MD simulations (black solid line) and the experimental S^2 values from the extended model is shown as a black dotted line. The positions of the helices (boxes) and β-strands (arrows) are indicated in each panel.

The generalized order parameter S^2, the asymptotic value of $C_i(t)$, represents another way to describe the restriction to reorientation of the NH vectors. S^2 takes values between 1 and 0. An S^2 value of 1 indicates complete restriction of the NH vector, whereas unrestricted motion yields S^2 values approaching 0. S^2(5 ns) is used to denote those order parameters obtained by considering the whole ensemble comprised of all structures from MD1 and MD2. If the $C_i(t)$ plots level to an asymptotic value, eq 3 yields a good estimate of the order parameters. However, for a MD simulation of finite length, this is not always the case, especially when a protein experiences motions that are too slow to be sampled adequately on the nanosecond time scale. For example, the NH vectors of Asn 33 jumped from one orientation to another at ~1700 ps. As demonstrated by Chandrasekhar et al. (*23*), the $C_i(t)$ for this kind of jumping motion will resemble two linear slopes with a break at ~800 ps (1700 + 800 = 2500 ps, the length of the simulation) (Figure 5). As a result, the $C_i(t)$ plot for Asn 33 drops linearly and yields a very low, and unreliable, S^2(5 ns) value. The problem is due to the fact that reorientation of the NH vectors on the nanosecond or slower time scale does not occur frequently enough to be sampled adequately in MD simulations that last for only several nanoseconds. For further discussion, see Chandrasekhar et al. (*23*).

On the other hand, the present MD simulations are long enough to reliably sample motions on a faster time scale (~100 ps). To describe internal motions on this time scale, S^2 order parameters were calculated with eq 3 with a window size of 250 ps (see Methods). S^2(250 ps) has several advantages over S^2(5 ns). First, it is statistically more reliable. The window size is $^1/_{10}$ of the length of a 2.5 ns trajectory, providing adequate sampling of motion faster than ~100 ps. Second, it falls closer to the time scale measured by NMR relaxation experiments. In summary, the two S^2 values, S^2(250 ps) and S^2(5 ns), describe motions on two different time scales. Although a quantitative interpretation of S^2(5 ns) is dangerous, it can be used as a qualitative indication of slower motions. If there is no internal motion on a time scale slower than ~100 ps, the two S^2 values should be equal. In fact, most residues have similar S^2 values derived for the two different window sizes (Figure 6A). On the other hand, a non-zero ΔS^2(250 ps−5 ns) value is indicative of the presence of slower motions (Figure 6A). Motion on a time scale slower than nanoseconds is manifested as a chemical exchange contribution on the transverse relaxation rate R_2 and line broadening of the resonances. It has been found that a large subset of residues in barstar C40/82A appear to undergo chemical exchange. Interestingly,

they correlate well with those residues with non-zero ΔS^2-(250 ps−5 ns) values (Figure 6A). In the following discussion, we will compare the more reliable S^2(250 ps) with S^2 from the NMR experiments.

Experimentally, the most popular model for analyzing NMR relaxation data is the "model-free" approach of Lipari and Szabo (*19*, *22*). The two model-free parameters derived, S^2 and τ_e, which is typically on the order of ∼100 ps, describe motions that are much faster than the overall tumbling. Comparison of S^2(250 ps) with S^2(NMR) reveals an offset difference. The average value of S^2(NMR) is 0.95 (*11*), whereas S^2(250 ps) is 0.84. As mentioned above, the $C_i(t)$ of backbone NH vectors tend to decay to ∼0.9 independent of the protein. From this point of view, the average S^2(NMR) value of 0.95 seems high. The fitting of relaxation data to the model-free formalism to obtain S^2 is sensitive to the overall correlation time, τ_m, chosen, which is not known a priori. Choosing a different τ_m will scale the S^2 values.

Another possible explanation for the high S^2 values from NMR might be the fact that the fitting of parameters to the original model did not explicitly consider the very fast phase of motion. The model-free formalism assumes that the $C_i(t)$ curves display a single-exponential decay with a time constant τ_e to an asymptotic value of S^2: $C_i(t) = S^2 + (1 - S^2)e^{-t/\tau_e}$. From the MD simulations, all the NH vectors experienced a sub-picosecond decay to ∼0.9. We have tried to account for this fast motion in interpreting the relaxation data by using the extended model-free formalism (*4*), which assumes that $C_i(t)$ can be fit as a double-exponential decay: $C_i(t) = S^2 + (1 - S^2)e^{-t/\tau_f} + (S_f^2 - S^2)e^{-t/\tau_s}$. In this case, S_f^2 corresponds to the amplitude of the sub-picosecond decay of $C_i(t)$ observed in the MD simulations and S^2 corresponds to S^2(250 ps) from the MD simulation. On the basis of the fact that $C_i(t)$ drops to 0.82−0.92 within the first 0.2 ps of the simulation, we set it as the bounds for S_f^2 and reoptimized the model-free parameters. The extended model predicts values of experimental relaxation rates similar to those of the original model analysis. The final optimized overall correlation time is slightly reduced from 5.8 to 5.5 ns. This leads to a slight offset of the S^2(NMR) values, resulting in S^2 values that are more consistent with those calculated from the MD simulations (Figure 6B). In any case, because of the necessity of fitting the experimental data, the absolute values can change but the comparison of the absolute values of S^2 is less important than the fact that both experiment and simulation indicate that the backbone NH vectors of barstar are relatively rigid on the ∼100 ps time scale, which is in contrast to the side chain dynamics.

Side Chain Dynamics. The dynamic behavior of methyl groups can be conveniently described by the reorientation of the symmetry axis of the CH_3 group. For example, for the methyl group of Thr, the reorientation of the $C_\beta-C_{\gamma 2}$ vector is monitored. In general, the CH vectors of the methyl groups in barstar cycle rapidly among the three equivalent sites about a symmetric axis. The average correlation time for methyl rotation was ∼39 ps, which falls within the range observed experimentally for the C−H vectors of leucine residues in staphylococcal nuclease, τ_f (5−80 ps) (*5*). In a manner similar to the approach outlined for the dynamics of backbone NH vectors, the autocorrelation functions and order parameters for the reorientation of the symmetry axes

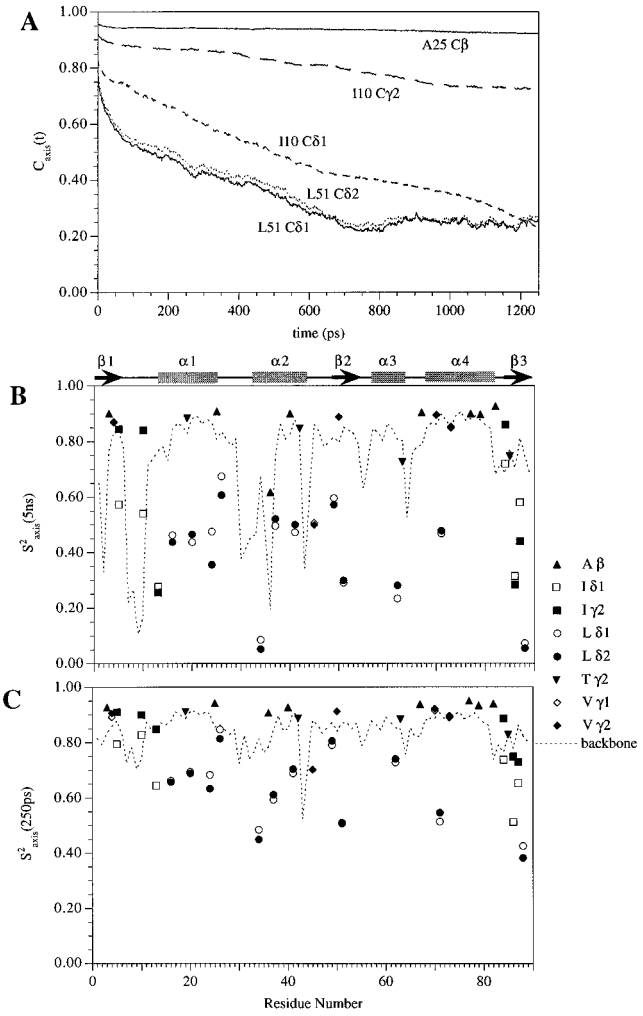

FIGURE 7: (A) Autocorrelation function for the symmetry axis of the methyl groups for some representative residues. The order parameters, S^2_{axis}, for the reorientation of the symmetry axis of the methyl groups were derived with eq 3 using two different window sizes: $T = 5$ ns (panel B) and $T = 250$ ps (panel C). The MD-derived S^2 values for the backbone NH vectors are shown as dotted lines.

were determined. Some examples of the autocorrelation functions for the methyl groups are shown in Figure 7A. The dynamics of the methyl side groups clearly depend on residue type. For alanine, the dynamics of the $C_\alpha-C_\beta$ vector was generally highly restricted and $C_i(t)$ dropped rapidly (<50 ps) and leveled off at approximately 0.9. For leucine and valine, the dynamic behavior of their methyl pairs was highly correlated. One representative example (the methyl pair of Leu 51) is shown in Figure 7A. On the other hand, the two methyl groups of isoleucine often had different dynamic properties. The $C_{\delta 1}$-methyl group of isoleucine is always more dynamic than the $C_{\gamma 2}$ counterpart (Figure 7A). This finding reflects the extra degree of freedom for $C_{\delta 1}$-methyls due to the rotation above the $C_\beta-C_{\gamma 1}$ axis.

Order parameters for the symmetry axis of the methyl groups (S^2_{axis}) were derived using eq 3. In an approach similar to the analysis of backbone dynamics, two values were calculated: S^2_{axis}(5 ns), using the whole ensemble of MD1 and MD2, and S^2_{axis}(250 ps), using a window size of 250 ps. The results are compared to the backbone S^2 values (Figure 7B). The dynamic behavior of the methyl groups is correlated with their separation from the backbone. That

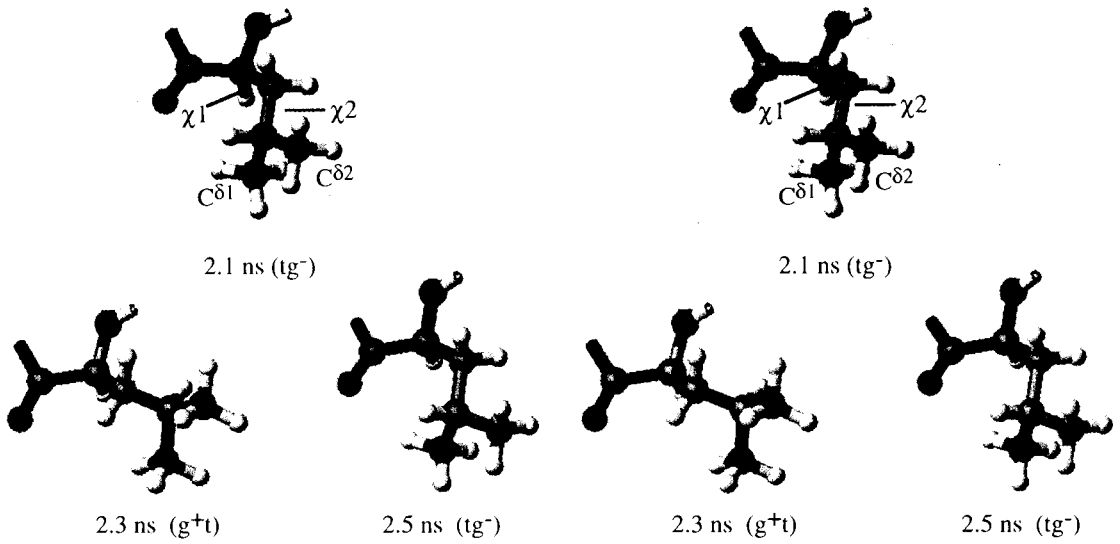

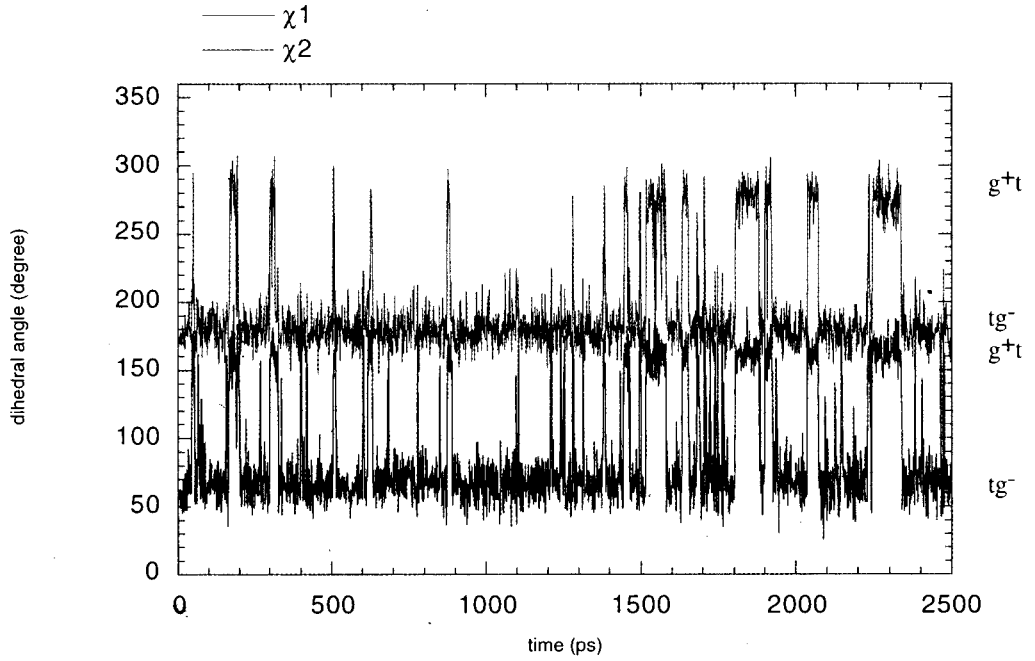

FIGURE 8: Demonstration of the hopping motion between the two predominant rotamers (tg^- and g^+t) of leucine residues. A representative case of Leu 71 is given. (A, top) Stereodiagram showing the structures of the two rotamers of leucine residues. Snapshots of structures for Leu 71 were taken from the MD2 simulation at various time points. $C_{\delta 1}$ and $C_{\delta 2}$ atoms are green and magenta, respectively, to show the swapping of the two methyl groups of leucine residues after the rotamer transition. (B, bottom) χ_1 (red line) and χ_2 (blue line) dihedral angles of Leu 71 are monitored as a function of simulation time. A number of $tg^- \rightarrow g^+t$ rotamer transitions was observed. This figure was created with MOLMOL (*53*).

is, alanine has the highest S^2 values, and the dynamics of the $C_\alpha - C_\beta$ vector is a reporter of backbone dynamics. For methyls at the C_γ position (Val, Thr, and Ile), the order parameters were generally high and close to the backbone value. On the other hand, methyls at the C_δ position (Leu and Ile) were more dynamic and deviated from their backbone values. In addition, comparison of S^2_{axis}(250 ps) and S^2_{axis}(5 ns) demonstrates that there was significant motion on both time scales, and in particular, the binding region and C terminus have very low S^2_{axis}(5 ns) values.

The methyl pairs of the leucine residues were more dynamic than those of other residues. Leucine residues were observed to undergo hopping motions between side chain rotamers. One representative example is Leu 71, as shown in Figure 8. The two expected populations of rotamers were observed. The mean χ_1 and χ_2 angles deviated slightly from the ideal angles (tg^-, $\chi_1 = 180°$ and $\chi_2 = 65°$; and g^+t, $\chi_1 = 285°$ and $\chi_2 = 165°$). The transition statistics are listed in Table 2. All leucine residues exhibited this hopping motion except Leu 26 and Leu 49, which had higher order parameters. This stereochemical property is unique to leucine residues, and the hopping between rotamers contributes to the lower order parameters observed for these methyl groups.

Table 2: Transition Statistics for Leucine Side Chain Rotamers[a]

residue	no. of transitions	g^+t lifetime (ps)	tg^- lifetime (ps)
16	19	36	410
20	6	1300	240
24	10	770	52
26	0	–	–
34	30	91	140
37	15	1.7	550
41	8	84	1000
49	0	–	–
51	24	19	280
62	3	1000	2100
71	46	16	180
88	22	190	96

[a] The rotamer conformation of a leucine residue is considered to be in the g^+t state if $\chi_1 = 285 \pm 30°$ and $\chi_2 = 165 \pm 30°$ or in the tg^- state if $\chi_1 = 180 \pm 30°$ and $\chi_2 = 65 \pm 30°$. The lifetime is the average time interval a leucine residue spends in the rotamer state before it undergoes a transition.

There are two Phe residues in barstar. Phe 74 is buried deep within the core, whereas Phe 56 is on the edge of the core. In the MD simulation, the aromatic ring of Phe 74 was found to flip rapidly, on the average undergoing one flip per 250 ps. No flipping of Phe 56 was observed.

DISCUSSION

We have simulated the structural and dynamic properties of barstar in solution. To ensure that the MD simulations provide realistic models for the behavior of barstar, we have put emphasis on comparison of MD-derived structural and dynamic parameters with those observed experimentally. Two 2.5 ns MD simulations of barstar were performed. The MD-generated ensemble of structures is generally consistent with the experimental NOEs, and no significant structural change was observed, suggesting that the MD simulations provide satisfactory models for the structure of barstar in solution. The following discussion focuses on the dynamic properties of barstar and implications for stability and function.

Backbone Dynamics on Different Time Scales. The dynamic behavior of individual bonds within barstar can be described by an autocorrelation function, $C(t)$, and a generalized order parameter, S^2, which can be readily extracted from the MD simulations. For MD simulations of a few nanoseconds, motions of time scales faster than ~100 ps are oversampled and can be readily compared with ^{15}N and ^{13}C NMR relaxation data. Motions on a range of time scales were observed in the barstar simulation presented here. A rapid drop of the autocorrelation function $C_i(t)$ to about 0.9 was found for all backbone NH vectors. The fast decay of $C_i(t)$ has also been observed in other MD simulations of proteins (*23*−*27*), and it corresponds to a small amplitude sub-picosecond motion that appears to be common to all NH bond vectors.

S^2(250 ps) was used to characterize motion on a time scale of ~100 ps for comparison with the experimentally derived S^2 values. As pointed out previously by Chandrasekhar et al. (*23*) and observed in the present MD simulations, the $C_i(t)$ values at later time points are statistically less reliable than those that oversample fast motion. An ensemble of two MD simulations of 2.5 ns each allows oversampling of the NH bond vector reorientation for yielding reliable values of S^2(250 ps). Indeed, S^2(250 ps) values calculated for MD1 and MD2 are similar (data not shown), indicating that both MD simulations sample the same fast motion (~100 ps) of the NH vectors.

The backbone of barstar is quite ordered, with S^2(250 ps) values between 0.7 and 0.9. The magnitude of the S^2(250 ps) values is correlated with the secondary structure elements. In particular, the backbone NH vectors in the helices often have very high S^2(250 ps) values (0.85−0.9), suggesting limited internal motion. On the other hand, the NH bond vectors on loop and turn regions have smaller S^2(250 ps) values (0.5−0.8), indicative of more extensive internal motion.

Barstar Has a Dynamic Hydrophobic Core. Side chain dynamics were evaluated by monitoring the symmetry axis of methyl groups and the flipping of aromatic side chains. Autocorrelation functions and order parameters S^2_{axis}(5 ns) and S^2_{axis}(250 ps) for the symmetry axis of the methyl groups were derived. Since the S^2_{axis}(5 ns) values have the same sampling problem as S^2(5 ns), our discussion will focus on S^2_{axis}(250 ps). In contrast to the relatively restricted backbone motion observed, the side chains exhibited a wide range of dynamic behavior, with S^2_{axis}(250 ps) ranging from 0.38 to 0.95. The dynamics of the side chain methyl groups were determined by residue type and their spatial separation from the main chain (Figure 7). The side chain dynamics of methyl groups can be studied by NMR spectroscopy (*5*−*9*). Models have been proposed for interpretation of the NMR relaxation data: (i) wobbling in a cone (*28*), (ii) restricted diffusion (*22*) (e.g., rotation about χ_1 for the methyl pairs of valine), and (iii) for methyl pairs of leucine residues, hopping between two predominant rotamers (*5*). All three mechanisms contributed to the internal motion of the methyl groups in the MD simulations of barstar. Among all methyl-containing residues, leucine was found to be the most mobile. The ability of the leucine side chain to readily jump between two rotamers may explain why these groups are more dynamic. In the crystal structures of proteins, leucine residues primarily adopt only two of the nine possible rotamers: tg^- ($\chi_1 \sim 180°$ and $\chi_2 \sim 60°$) and g^+t ($\chi_1 \sim 300°$ and $\chi_2 \sim 180°$) (*29*). Solid-state ^2H NMR studies have shown that the two conformations can interconvert rapidly ($t < 10^{-7}$ s) (*30*−*32*). In the present MD simulations, 10 out of 12 leucine residues were found to exhibit hopping between rotamers. This structural rearrangement of the leucine residues swaps the positions of the $C_{\delta 1}$ and $C_{\delta 2}$ methyl groups without a large distortion of the backbone conformation and the hydrophobic side chain packing is maintained (Figure 8).

Although ^{13}C relaxation data are not available for barstar, a number of ^{13}C relaxation studies of other proteins have suggested that the internal motion of core residues can be substantial. Pioneering studies of side chain dynamics of myoglobin (*33*) and BPTI (*34*) demonstrated significant internal motion of the methyl groups along the symmetry axis for a number of large hydrophobic residues. In recent relaxation studies of staphylococcal nuclease (*5*), the C-terminal SH2 domain from phospholipase Cγ1 (PLCC) (*8*), ubiquitin (*9*), and thioredoxin (*6*), the methyl groups display a wide range of dynamics, from being almost unrestricted to completely restricted (with experimental S^2_{axis} values ranging from 0.1 to 1). A number of these mobile side chains

Table 3: Comparison of the Methyl Dynamics of Barstar with Those of Other Proteins As Measured by S^2_{axis}[a]

methyl group	barstar (MD)[b]	PLCC (NMR)[c]	ubiquitin (NMR)[d]	staphylococcal nuclease (NMR)[e]
Ala	0.90−0.95 (0.93)	0.22−92 (0.76)	0.09−0.72 (0.41)	−
Ile δ1	0.51−0.83 (0.69)	0.37−0.62 (0.46)	0.45−0.99 (0.73)	−
Ile γ2	0.73−0.91 (0.84)	0.63−0.94 (0.75)	0.27−1 (0.80)	−
Leu δ1	0.43−0.85 (0.63)	0.20−0.83 (0.52)	0.27−1 (0.73)	0.32−0.90 (0.64)
Leu δ2	0.38−0.81 (0.63)	0.20−0.81 (0.50)	0.27−0.99 (0.55)	0.33−0.90 (0.59)
Thr	0.83−0.91 (0.88)	0.42−0.83 (0.62)	0.45−0.99 (0.81)	−
Val γ1	0.70−0.91 (0.86)	0.31−0.63 (0.49)	0.63−1 (0.78)	−
Val γ2	0.70−0.92 (0.87)	0.33−0.83 (0.50)	0.18−1 (0.75)	−
Met	−	0.12−0.26 (0.18)	−	−

[a] Averaged S^2_{axis} values are shown in parentheses. [b] S^2_{axis}(250 ps) derived from the MD simulations. [c] Data for unbound PLCC are from Kay et al. (*8*). [d] S^2_{axis} was calculated from the data of Wand et al. (*9*) as follows: $S^2_{axis} = S^2/0.111$. For S^2 values greater than the Woessner limit of 0.111, S^2_{axis} values were assumed to be 1. [e] S^2_{axis} for Leu residues of staphylococcal nuclease were obtained from Nicholson et al. (*5*).

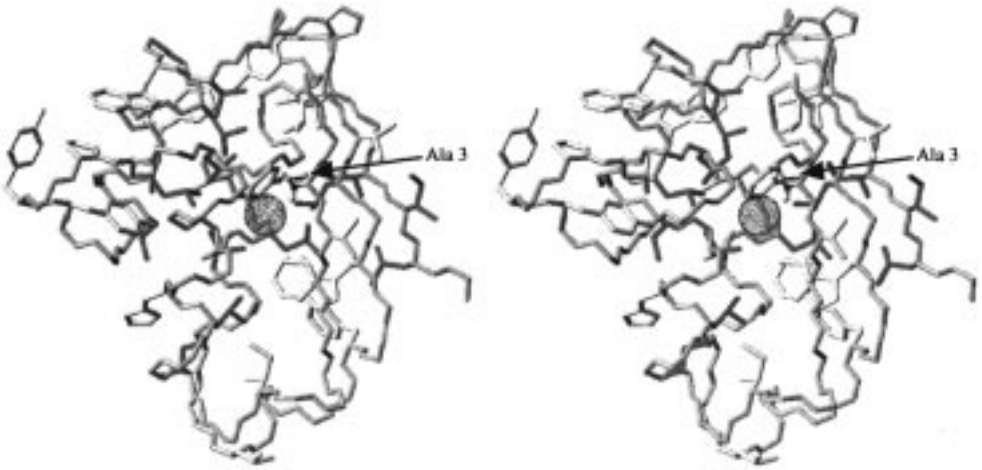

FIGURE 9: Stereodiagram showing the hydrophobic side chains of barstar. Mobile methyl side chains with S^2_{axis} values of $\leq$0.7 are red (Ile 13, 86, and 87, Leu 16, 20, 24, 34, 37, 41, 51, 71, and 88, and Val 45). Phe 74, which experienced ring flipping, is gold. Other side chains are gray. The program SURFNET (*54*) was used to identify cavities in the NMR structures. Note that a cavity (black dotted sphere) in the hydrophobic core was found near Ala 3 (shown as a ball-and-stick model). This figure was created with MOLMOL (*53*).

are buried within the hydrophobic core. This observation is in contrast to the relatively restricted NH backbone dynamics, with typical S^2 values ranging from 0.7 to 0.9 (*3*). A comparison of S^2_{axis} values of barstar derived with MD simulation with the experimental S^2_{axis} values for the proteins mentioned above is shown in Table 3. Despite the fact that different proteins can have distinct dynamic properties, it appears that the S^2_{axis} values for barstar are reasonable and fall into the range observed for other proteins by NMR. As shown in Figure 9, most of the mobile methyl side chains ($S^2_{axis} \leq 0.7$) are buried within the hydrophobic core.

Other evidence suggesting that barstar has a dynamic core is provided by the flipping of the aromatic ring of Phe 74. The protons at the δ and ϵ positions of Phe 56 and Phe 74 of wild-type barstar (*10*) and the C40/82A mutant (*11*) have degenerate chemical shifts. The degeneracy can be explained by a similar chemical environment around the hydrogens or the aromatic ring may be flipping rapidly such that the chemical shifts report on the average chemical environment surrounding the ring. To investigate the first possibility, we have used Osapay and Case's SHIFT program (*35*) to predict whether the intrinsic chemical shift differences between the pairs of symmetric ring protons are significant (Phe 56, H^δ 1.46 and H^ϵ 0.51; and Phe 74, H^δ 0.56 and H^ϵ 0.08). These values suggest that the differences are meaningful and that both the aromatic rings are flipping rapidly on the chemical shift time scale ($\gg 10^3$ s^{-1}, or at least one flip per $\sim$10 ms). It should be noted that MD simulations that last for several nanoseconds may not be able to observe such ring flipping. Here the aromatic ring of Phe 74 was found to flip rapidly, but that of Phe 56 was not. Phe 56 is on the edge of the core, whereas Phe 74 is buried deeply inside the hydrophobic core and is inaccessible to solvent. The fact that Phe 74 flips rapidly on a nanosecond time scale suggests that the hydrophobic core must be very dynamic.

The mobile core side chains are displayed in Figure 9. Globular proteins are generally densely packed (*36*). However, a number of core residues in barstar are very dynamic. Structural rearrangements such as ring flipping and hopping motions of the leucine residues were observed. These findings are not compatible with the view that a hydrophobic core is rigid and that rearrangement inevitably causes steric clashes. Hydrophobic cores, like this one, may be better described as a liquid phase where energetic barriers among substates are low and there is a larger degree of freedom associated with the side chains.

A high leucine content may be one of the clues as to why barstar has a fluid hydrophobic core. The leucine content in the core of barstar is double that of other small globular proteins (<200 amino acids) (Figure 10), and leucine side chains can readily interconvert between rotamers with preservation of packing. Another clue is that the core of barstar has packing defects and/or cavities that can accommodate transient changes in conformation due to heightened

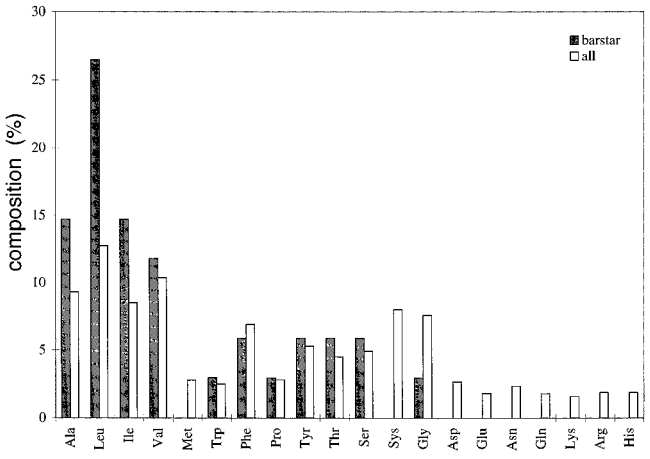

FIGURE 10: Comparison of the composition of the hydrophobic core residues of barstar with other small proteins. The nonredundant list of PDB files was obtained from Hobohm and Sander (*55*). Only proteins smaller than 200 residues were included. Core residues were defined as those with less than 25% solvent accessible surface (relative to those in an extended Ala-X-Ala tripeptide; *56*). The solvent accessible surface area was calculated using the program NACCESS (*57*). Note that the leucine residues constitute 26% of the total number of core residues in barstar, compared with 13% for other proteins.

mobility. One such cavity is in the vicinity of Ala 3 (Figure 9). It would be interesting to mutate Ala 3 to a residue with a longer side chain, to fill the cavity and see if there is any change in the dynamic behavior of the protein.

Dynamics and Stability. There is not a clear and definitive link between dynamics of the hydrophobic core and the stability of proteins. Studies of BPTI and its derivatives suggest that the rate of ring flipping and methyl dynamics are not correlated with stability (*37*). However, in a study of Trp side chain dynamics of chymotrypsin inhibitor 2, a weak correlation was found between mobility and protein stability (*38*). Equilibrium studies indicate that barstar has unusual thermodynamic properties for its size; it has an unusually low enthalpy, ΔH, and low entropy, ΔS, of unfolding, as well as a high heat capacity increment of unfolding, ΔC_p [at 298 K, $\Delta H = 4.0$ kcal/mol, $\Delta C_p = 1.46$ kcal mol^{-1} K^{-1} (*39*); $\Delta G = 4.84$ kcal/mol (*40*)]. Wintrode et al. (*41*) estimated the contribution of hydration and internal interactions to ΔH and ΔS of unfolding and suggest that the low enthalpy of unfolding may be due to weak interactions within the hydrophobic core in the native state. One possible explanation is that packing defects in the core of barstar lower the enthalpy and allow for significant internal motion of the core residues. A more dynamic core then increases the entropy of the native state. As a result, there would be only a small increase in entropy upon unfolding, as is observed. Such findings may have important implications for the interpretation of thermodynamic data, in that the entropy of the native state cannot be neglected, as has also been suggested by Li et al. (*42*), Wand et al. (*9*), and Yang and Kay (*43*). In addition, we note that the entropy of the native state is generally considered to be low or negligible and stability is usually rationalized in terms of enthalpy of the native state and entropy of the denatured state; increasing the entropy of the native state without substantial disruptions of favorable enthalpic interactions represents another possible route for lowering the free energy and thereby stabilizing the native state. Conformational degeneracy may be important in not only determining and stabilizing the native state but also improving the odds during folding.

Dynamics and Function. Motion is a necessary consequence of thermal energy, but it may also be critical to function and designed into a protein. In general terms, conformational substates may be important to function. For example, on the basis of studies of ligand binding to myoglobin, Hong et al. (*44*) suggested that conformational substates near the native state can perform the same function but at different rates [see Kazmirski and Daggett (*45*) for further discussion and other examples]. Also, specific regions of heightened mobility along the sequence are often associated with function. The first direct experimental correlation between dynamics and activity came from NMR relaxation studies of dihydrofolate reductase and folate by Epstein et al. (*46*). They found that regions of the structure involved in transition-state stabilization and ligand-dependent conformational changes were particularly mobile. Barstar is much simpler; its function is to bind to and inhibit the ribonuclease barnase.

The interaction of barstar and barnase is mainly electrostatic in nature (*12*, *47*). Residues involved in binding are located primarily in the binding loop (between helices 1 and 2) and helix 2 (Figure 1). Structural changes of barstar upon binding to barnase involve side chain rotations of Asp 35 and Asp 39 as well as movement of the binding loop which brings Tyr 29 into the active site of barnase (*11*, *12*). Interestingly, NMR relaxation data suggest that the backbone of the binding loop and the N terminus of helix 2 exhibit chemical exchange on the microsecond to millisecond time scale, and the simulations also provide evidence for heightened mobility in these areas on the nanosecond but not on the picosecond time scale (Figures 6 and 7). This localized flexibility may aid in the docking of the binding loop and helix 2 to the active site of barnase. As shown by *B* factors in the crystal structure of barstar bound to barnase, there is a loss of flexibility in this binding region upon interaction with barnase. This effect suggests that flexibility is important for the interaction between the two proteins. More conclusive evidence would be provided by molecular dynamics simulations of the complex and a comparison with the dynamic behavior of the unbound components.

CONCLUDING REMARKS

We performed MD simulations to study the backbone and side chain dynamics of barstar. While the backbone is relatively rigid, the side chains experienced a wide range of dynamic behavior. Many of these mobile side chains constitute the hydrophobic core of barstar. This finding implies that the hydrophobic core is very dynamic and is best described as fluid-like with low energy barriers between substates. Structural rearrangements such as the hopping motion of the leucine side chains and flipping of an aromatic ring were prevalent and occurred without a significant change in the backbone conformation, suggesting that the hydrophobic core of barstar can easily accommodate alternative packing arrangements. The plasticity of the hydrophobic interior has also been demonstrated by mutagenesis of the core residues of other proteins, including the N-terminal domain of the λ-repressor (*48*, *49*), T4 lyzozyme (*50*), and barnase (*51*). While barstar may be more dynamic than most

proteins due to its high leucine content and packing defects, on the basis of comparisons with other proteins, it is probably not qualitatively atypical.

Our MD simulations also suggest that considering either backbone or side chain dynamics alone can yield a quite different description of the dynamic behavior of a protein. If the dynamics can be equated with residual entropy, it is the side chain motion that makes the biggest contribution. Thus, it would be incomplete to interpret dynamic behavior, or entropy, of a protein solely on the basis of backbone dynamics. Another implication of these results is that the entropy of the native state may play an important role in the thermodynamic properties of a protein and cannot be neglected. A static picture offered by the mean coordinates can be merely incomplete or on the verge of misleading. Therefore, characterization of both the dynamic and structural properties of a protein is crucial to understanding stability and function.

ACKNOWLEDGMENT

We thank Drs. A. Szabo and A. J. Wand for stimulating discussions and helpful comments on the manuscript.

REFERENCES

1. Palmer, A. G. (1997) *Curr. Opin. Struct. Biol. 7*, 732−737.
2. Wagner, G. (1993) *Curr. Opin. Struct. Biol. 3*, 748−754.
3. Kay, L. E., Torchia, D. A., and Bax, A. (1989) *Biochemistry 28*, 8972−8979.
4. Clore, G. M., Driscoll, P. C., Wingfield, P. T., and Gronenborn, A. M. (1990) *Biochemistry 29*, 7387−7401.
5. Nicholson, L. K., Kay, L. E., Baldisseri, D. M., Arango, J., Young, P. E., Bax, A., and Torchia, D. A. (1992) *Biochemistry 31*, 5253−5263.
6. LeMaster, D. M., and Kushlan, D. M. (1996) *J. Am. Chem. Soc. 118*, 9255−9264.
7. Muhandiram, D. R., Yamazaki, T., Sykes, B. D., and Kay, L. E. (1995) *J. Am. Chem. Soc. 117*, 11536−11544.
8. Kay, L. E., Muhandiram, D. R., Farrow, N. A., Aubin, Y., and Forman-Kay, J. D. (1996) *Biochemistry 35*, 361−368.
9. Wand, A. J., Urbauer, J. L., McEvoy, R. P., and Bieber, R. J. (1996) *Biochemistry 35*, 6116−6125.
10. Lubienski, M. J., Bycroft, M., Freund, S. M. V., and Fersht, A. R. (1994) *Biochemistry 33*, 8866−8877.
11. Wong, K., Fersht, A., and Freund, S. (1997) *J. Mol. Biol. 268*, 494−511.
12. Buckle, A. M., Schreiber, G., and Fersht, A. R. (1994) *Biochemistry 33*, 8878−8889.
13. Guillet, V., Lapthorn, A., Hartley, R. W., and Mauguen, Y. (1993) *Structure 1*, 165−177.
14. Levitt, M. (1990) *ENCAD*, Molecular Applications Group, Palo Alto, CA, and Yeda, Rehovot, Israel.
15. Levitt, M., Hirshberg, M., Sharon, R., and Daggett, V. (1995) *Comput. Phys. Commun. 91*, 215−231.
16. Levitt, M., Hirshberg, M., Sharon, R., Laidig, K., and Daggett, V. (1997) *J. Phys. Chem. 101*, 5051−5061.
17. Kell, G. S. (1967) *J. Chem. Eng. Data 12*, 66−69.
18. Kabsch, W. (1976) *Acta Crystallogr. 32A*, 922−923.
19. Lipari, G., and Szabo, A. (1982) *J. Am. Chem. Soc. 104*, 4546−4559.
20. Levitt, M. (1983) *J. Mol. Biol. 168*, 621−657.
21. Abragam, A. (1961) *The principles of nuclear magnetism*, Clarendon Press, Oxford, England.
22. Lipari, G., and Szabo, A. (1982) *J. Am. Chem. Soc. 104*, 4559−4570.
23. Chandrasekhar, I., Clore, G., Szabo, A., Gronenborn, A., and Brooks, B. (1992) *J. Mol. Biol. 226*, 239−250.
24. Eriksson, M., Berglund, H., Härd, T., and Nilsson, L. (1993) *Proteins 17*, 375−390.
25. Philippopoulos, M., and Lim, C. (1995) *J. Mol. Biol. 254*, 771−792.
26. Smith, P., van Schaik, R., Szyperski, T., Wüthrich, K., and van Gunsteren, W. (1995) *J. Mol. Biol. 246*, 356−365.
27. Yamasaki, K., Saito, M., Oobatake, M., and Kanaya, S. (1995) *Biochemistry 34*, 6587−6601.
28. Woessner, D. (1962) *J. Chem. Phys. 36*, 1−4.
29. Janin, J., Wodak, S., Levitt, M., and Maigret, B. (1978) *J. Mol. Biol. 125*, 357−386.
30. Batchelder, L., Sullivan, C., Jelinski, L., and Torchia, D. (1982) *Proc. Natl. Acad. Sci. U.S.A. 79*, 386−389.
31. Colnago, L., Valentine, K., and Opella, S. (1987) *Biochemistry 26*, 847−854.
32. Leo, G., Colnago, L., Valentine, K., and Opella, S. (1987) *Biochemistry 26*, 854−862.
33. Jones, W., Jr., Rothgeb, T., and Gurd, F. (1976) *J. Biol. Chem. 251*, 7452−7460.
34. Richarz, R., Nagayama, K., and Wüthrich, K. (1980) *Biochemistry 19*, 5189−5196.
35. Osapay, K., and Case, D. A. (1991) *J. Am. Chem. Soc. 113*, 9436−9444.
36. Richards, F. (1974) *J. Mol. Biol. 82*, 1−14.
37. Wüthrich, K., Wagner, G., Richarz, R., and Braun, W. (1980) *Biophys. J. 32*, 549−560.
38. Matthews, S., Jandu, S., and Leatherbarrow, R. (1993) *Biochemistry 32*, 657−662.
39. Agashe, V. R., and Udgaonkar, J. B. (1995) *Biochemistry 34*, 3286−3299.
40. Schreiber, G., and Fersht, A. R. (1993) *Biochemistry 32*, 11195−11203.
41. Wintrode, P. L., Griko, Y. V., and Privalov, P. L. (1995) *Protein Sci. 4*, 1528−1534.
42. Li, Z., Raychaudhuri, S., and Wand, A. J. (1996) *Protein Sci. 5*, 2647−2650.
43. Yang, D., and Kay, L. E. (1996) *J. Mol. Biol. 263*, 369−382.
44. Hong, M. K., Braunstein, D., Cowen, B. R., Frauenfelder, H., Iben, I. E. T., Mourant, J. R., Ormos, P., Scholl, R., Schulten, A., Steinbach, P. J., Xie, A.-H., and Young, R. D. (1990) *Biophys. J. 58*, 429−436.
45. Kazmirski, S. L., and Daggett, V. (1997) *Adv. Mol. Cell Biol. 22B*, 339−390.
46. Epstein, D. M., Benkovic, S. J., and Wright, P. E. (1995) *Biochemistry 34*, 11037−11048.
47. Schreiber, G., and Fersht, A. (1996) *Nat. Struct. Biol. 3*, 427−431.
48. Lim, W., and Sauer, R. (1989) *Nature 339*, 31−36.
49. Lim, W., and Sauer, R. (1991) *J. Mol. Biol. 219*, 359−376.
50. Gassner, N., Baase, W., and Matthews, B. (1996) *Proc. Natl. Acad. Sci. U.S.A. 93*, 12155−12158.
51. Axe, D., Foster, N., and Fersht, A. (1996) *Proc. Natl. Acad. Sci. U.S.A. 93*, 5590−5594.
52. Kraulis, P. J. (1991) *J. Appl. Crystallogr. 24*, 946−950.
53. Koradi, R., Billeter, M., and Wüthrich, K. (1996) *J. Mol. Graphics 14*, 51−55.
54. Laskowski, R. (1995) *J. Mol. Graphics 13*, 323−330.
55. Hobohm, U., and Sander, C. (1994) *Protein Sci. 3*, 522−524.
56. Hubbard, S., Campbell, S., and Thornton, J. (1991) *J. Mol. Biol. 220*, 507−530.
57. Hubbard, S. J., and Thornton, J. M. (1993) *NACCESS*, Department of Biochemistry and Molecular Biology, University College, London.

BI980552I